A Comparison of Mesoscale Eddy Heat Fluxes from Observations and a High-Resolution Ocean Model Simulation of the Kuroshio Extension

Stuart P. Bishop * and Frank O. Bryan

National Center for Atmospheric Research, Boulder, CO

* *Corresponding author address:* National Center for Atmospheric Research, Boulder, CO 80307

E-mail: sbishop@ucar.edu

ABSTRACT

For the first time estimates of divergent eddy heat flux (DEHF) from a high-resolution (HR, 0.1°) simulation of the Parallel Ocean Program (POP) are compared with estimates made during the Kuroshio Extension System Study (KESS). The results from POP are in good agreement with KESS observations. POP captures the lateral and vertical structure of mean-to-eddy energy conversion rates, which range from 2–10 $cm^2\ s^{-3}$. The dynamical mechanism of vertical coupling between the deep and upper ocean is the process responsible for DEHFs in POP and is in accordance with baroclinic instability observed in the Gulf Stream and Kuroshio Extension. Meridional eddy heat transport values are ∼14% larger in POP at its maximum value. This is likely due to the more zonal path configuration in POP. The results from this study suggest that HR POP is a useful tool for estimating eddy statistics in the Kuroshio Extension region, and thereby provide guidance in the formulation and testing of eddy mixing parameterizations schemes.

1. Introduction

Mesoscale eddies with length scales O(10–100 km) arising from instabilities of the time mean flow are a ubiquitous feature of the ocean circulation. Motions on these scales account for the majority of the kinetic energy of the flow, with maximum eddy kinetic energy (EKE) found in the regions surrounding western boundary currents and their extensions, and the Antarctic Circumpolar Current. The eddies are more than just noise, they are integral to the dynamical balances, and energy and material transport throughout the ocean. Therefore, ocean models used in climate simulation must represent the effects of eddies on the mean flow and account for their transport properties. High-resolution (HR) ocean models have begun to resolve these scales (Hecht and Hasumi 2008), and a few coupled climate simulations have been conducted with ocean models of this class (McClean et al. 2011; Kirtman et al. 2012). In order to quantify the uncertainty in these simulations, it is important to establish the degree of fidelity of HR ocean models in representing eddy-mean flow interaction processes. While a number of studies have evaluated the ability of HR models to reproduce the observed geographical distribution of eddy energy or near surface fluxes of heat or momentum, e.g. (McClean et al. 2006; Lenn et al. 2011), validation of the eddy-resolving models in terms of the three-dimensional structure of eddy covariances (*e.g.* heat flux) is difficult because of the general lack of ocean observations at sufficient spatial resolution and the long sampling requirements for statistical convergence (Flierl and McWilliams 1977).

Observations from the Kuroshio Extension System Study (KESS) offer a unique data set to test the validity of HR model outputs. KESS was a multi-institutional field program from 2004-2006, which was comprised of an observational array of current and pressure equipped inverted echo sounders (CPIES) and eight subsurface moorings. The subsurface moorings were located between the first quasi-stationary meander crest and trough east of Japan in the region of highest EKE (Jayne et al. 2009). The geostrophic currents and temperature field derived from the CPIES observations agreed well with the subsurface moorings (Donohue et al. 2010). The CPIES data was further used to estimate eddy heat flux and this estimate agreed with estimates at the locations of the subsurface moorings (Bishop et al. 2013).

Transient eddy heat fluxes in the ocean and atmosphere have large rotational (nondivergent) components that do not play a role in eddy-mean flow interactions and mask the smaller, but important, divergent component. For this reason, it is necessary to distinguish between rotational and divergent components; see (Marshall and Shutts 1981; Jayne and Marotzke 2002; Fox-Kemper et al. 2003) for further discussion. The objective of this study is to compare estimates of divergent eddy heat flux (DEHF) from KESS CPIES observations with those from an eddy-resolving integration of the Parallel Ocean Program (POP) developed at Los Alamos National Laboratory. To our knowledge, this is the first time the magnitude and three-dimensional structure of the dynamically active divergent component of simulated eddy heat fluxes have been directly evaluated using observations. In addition, we compare mechanisms responsible for generation of the eddies that give rise to DEHF.

Beyond the direct evaluation of this particular simulation, establishing the fidelity of HR models has broader implications for climate model development. Current generation global ocean climate models do not resolve mesoscale eddies, and will not be able to do so routinely for some time. Climate models use parameterizations to include the effects of unresolved scales (*e.g.* Gent and McWilliams (1990), GM90 hereafter) where eddy heat fluxes are represented as a flux-gradient relationship proportional to an eddy diffusivity. These parameterizations are often tested against higher-resolution eddy-resolving simulations (Fox-Kemper et al. in press). By establishing the fidelity of the eddy-resolving simulation, we can therefore provide a firmer basis for testing of a broad class of climate models.

In the next section the model and observational data sets will be described. Additionally, the methods for estimating DEHF and a means of comparison between the two data sets will be described. The following sections will present the results of the model-observation comparison followed by a discussion and conclusions.

2. Methods

a. KESS Observations

The KESS array provided full maps twice daily of geostrophic current and temperature for 16 months from June 2004 to September 2005, after which some CPIES stopped working (the processing of the CPIES maps are documented in Donohue et al. (2010)). Geostrophic currents determined from the CPIES separate the vertical structure into an equivalent-barotropic internal mode ($\mathbf{u}_I$) and a nearly depth-independent external mode ($\mathbf{u}_E$). The internal mode geostrophic current profiles were estimated from the mapped geopotential (Φ),

$$f\mathbf{u}_I = \mathbf{k} \times \nabla\Phi, \tag{1}$$

referenced to 5300 dbar, where f is the Coriolis parameter, $\mathbf{k}$ is the vertical unit vector aligned with the gravitational acceleration, and $\nabla = (\partial/\partial x, \partial/\partial y)$ is the horizontal gradient operator. Measurements from the current meters and pressure gauges at the bottom provided the external mode and reference current at 5300 dbar, $\mathbf{u}_E$, that is nearly depth-independent away from steep topography (Bishop et al. 2012) to establish absolute geostrophic current profiles,

$$\mathbf{u} = \mathbf{u}_I + \mathbf{u}_E. \tag{2}$$

The external mode, $\mathbf{u}_E$, may cross the front, causing the vector sum total current to veer or back with depth, which drives cross-frontal and vertical motion along sloping isopycnals (Lindstrom et al. 1997).

To match the POP model outputs described in the next section, the current and temperature maps were 5-day averaged. The cross-spectral energy of v_E and T at time-scales less than 10 days is small (Bishop 2013, 2012), suggesting that there is little loss of energy by 5-day averaging.

b. POP Model Data

The model used is POP, a general circulation model that solves the three-dimensional primitive equations. The model configuration for the simulation used in this study is the same as in Maltrud et al. (2010) and Douglass et al. (2012a,b). The model has a global tripole grid with horizontal resolution $0.1° \times \cos(\text{latitude})$ in both the zonal and meridional directions, which is sufficient to resolve the most energetic scales of mesoscale variability. In the vertical, the model has 42 levels, with vertical spacing of 10 m near the ocean surface and stretching to 250 m below 1000 m depth. The model experiment was run for 120 years with annually-repeating surface atmospheric forcing, downward radiative fluxes, and precipitation from a climatology blending of the National Center of Environmental Prediction reanalysis product and remote sensing products (Large and Yeager 2009). The outputs saved for this run were monthly-averaged potential temperature, salinity, and velocity, but 5-day-averaged variables were saved for model years 64–67. The potential temperature and horizontal velocity field from years 64–67 are used in this study because monthly outputs would underestimate a large fraction of the eddy variability observed in the 30–60 day band (Greene et al. 2012). To match the KESS observations, only the region between 143°–149°E and 32°–39°N is considered.

c. Divergent Eddy Heat Flux

Eddy heat flux is defined as the temporal correlation between the horizontal current and temperature field, $\overline{\mathbf{u}'T'}$ where $\mathbf{u} = (u, v)$ is the horizontal current, T is the potential temperature, a bar indicates a time mean, and primes indicate a deviation from the time mean. When studying eddy heat fluxes, it is important to distinguish between rotational (nondivergent) and divergent components (Marshall and Shutts 1981). It is the divergent component that plays a role in eddy-mean flow interactions.

In the Kuroshio Extension a very different picture emerges when the distinction between rotational and divergent fluxes is made (Bishop et al. 2013). For the CPIES data set the eddy heat flux associated with $\mathbf{u}_I$, which does not advect the temperature field, is completely rotational and proportional to temperature variance contours (Marshall and Shutts 1981). The eddy heat flux due to $\mathbf{u}_E$, which can advect the temperature field, is responsible for driving DEHFs. However, $\overline{\mathbf{u}'_E T'}$ is not rotation free. The divergent component is then determined by removing the best-fit rotational component determined from Objective Analysis (OA) (see Bishop et al. (2013) and Watts and Tracey (2013) for details of this method),

$$\overline{\mathbf{u}'T'}^{div} = \overline{\mathbf{u}'_E T'} - \overline{\mathbf{u}'_E T'}^{OA}. \tag{3}$$

For the POP data, $\mathbf{u}_E$ was chosen to be the velocity at 5125 m, which is close to the CPIES data (5300 dbar). The mean vertical shear along the jet path in the model data below 1500 m is $O(10^{-5})$ s^{-1}, which is ∼1% of the vertical shear within the thermocline, such that the deep currents are mostly uniform with depth. $\overline{\mathbf{u}'_E T'}$ was then estimated in a manner consistent with the model numerics. It was confirmed that the model upper ocean eddy heat flux due to the full velocity field, $\overline{\mathbf{u}'T'}$, was mostly rotational and proportional to temperature variance contours (not shown), similar to observations (Bishop et al. 2013).

To determine the agreement of the POP model with the CPIES observations, two metrics will be compared: the mean-to-eddy energy conversion rates and meridional eddy heat transport (MEHT). The mechanism of vertical coupling between the deep and upper ocean, responsible for DEHFs in the Kuroshio Extension and Gulf Stream, will also be tested in POP.

1) Energy Conversion

The mean-to-eddy energy conversion rates are estimated from

$$BC = -\frac{\alpha g}{\Theta_z}\overline{\mathbf{u}'T'}^{div} \cdot \nabla\overline{T} \tag{4}$$

where α is the effective expansion coefficient $O(10^{-4\circ}C^{-1})$ (Hall 1986; Cronin and Watts 1996; Phillips and Rintoul 2000), g is the gravitational acceleration, and Θ_z is the regionallyaveraged potential temperature gradient. BC is termed the baroclinic conversion (Cronin and Watts 1996), which when positive is a measure of the energy conversion from mean potential energy to eddy potential energy. Positive BC is indicative of baroclinic instability processes in the ocean and is the foundation for the GM90 parameterization.

2) Meridional Eddy Heat Transport

MEHT is estimated by vertically- and zonally-integrating the divergent meridional eddy heat flux,

$$Q = \rho_0 C_p \int_0^L \int_{-H}^0 \overline{v'T'}^{div} dz dx \tag{5}$$

where ρ_0 is the regional depth-averaged density of 1027.5 kg m^{-3}, C_p is the specific heat at constant pressure for seawater at $\sim$ 4000 J kg^{-1} °C^{-1}, and x and z are the zonal and vertical coordinates respectively. Equation (5) is vertically integrated from 100–5000 m depth and zonally integrated from 143.5°–148.5°E.

3. Results

a. Energy Conversion

The DEHF vectors and energy conversion rates (Eq. 4) at mid-thermocline depth for KESS and POP are shown in Figures 1a,b respectively. The cross-stream DEHF vectors are also comparable with values 5–12 cm s^{-1} °C. For both KESS and POP, the DEHF is directed west and south in the area south of the meander crest, and east and south in the area south of the meander trough. The DEHFs north of the jet are relatively weaker in magnitude than those to the south for both. The conversion rates are comparable and predominately positive (2–10 cm^2 s^{-3}) in both data sets. BC has a similar spatial structure in both data sets with large down-gradient DEHFs concentrated near the jet mean path between a crest and trough. The mean jet path in POP is shifted $\sim$0.5° north, which explains why the large energy conversion rates in POP are more north than the KESS observations. It is a common problem in ocean general circulation models that the Western Boundary Current (WBC) extensions (*e.g.* Gulf Stream and Kuroshio Extension) tend to take a more poleward path (Chassignet and Marshall 2008).

Since there is the offset in latitudinal dependence of the energy conversion, BC was zonally averaged along mean temperature contours (Figure 1c). The mean temperature contours are pseudo streamlines since the flow is approximately equivalent barotropic. BC reaches a maximum along the 11°C isotherm in both data sets (4.73×10^{-3} cm^2 s^{-3} in KESS and 3.46×10^{-3} cm^2 s^{-3} in POP). Thus, the maximum BC is 27% smaller in POP along the 11°C, but it has a broader latitudinal structure.

The vertical structures of the energy conversion rates are also comparable. The vertical structure of BC along the axis of the jet (defined as the 11°C isotherm at 400 m depth) is shown in Figure 2. BC reaches a maximum near 145.5°E and 400 m depth in both KESS and POP (Figures 2a and 2b). It is mainly in the upper ocean (200–500 m depth) that POP underestimates BC (Figure 2c). The vertical structure is similar on other temperature isotherms surrounding the 11°C isotherm (not shown).

b. Vertical Coupling

Vertical coupling between the deep and upper ocean is the dynamical mechanism that drives DEHFs in WBC extensions and to the subsequent release of available potential energy of the mean jet (Bishop 2013; Cronin and Watts 1996). Fig. 3a shows 5-day snap shots of the vertical coupling between the deep and upper ocean in POP during the formation of a cold-core ring (CCR). As the trough steepens in the mid-thermocline temperature field at 381 m there are deep current vectors at 5125, $\mathbf{u}_E$, that cross the front; exhibiting very different behavior from equivalent barotropicity. These deep currents are associated with lows and highs shown by the streamfunction, ψ_E. Fig. 3b shows that the POP deep field is leading the mid-thermocline temperature field by $\sim$7 days, with joint growth in the 30–60 day band (compared with 8 days in KESS (Bishop 2013)). The joint growth of the deep and thermocline fields in the 30–60 day band is consistent with the canonical view of the 2-layer Phillips model of baroclinic instability and has been observed in the Gulf Stream (Cronin and Watts 1996) and Kuroshio Extension (Bishop 2013; Tracey et al. 2012). The 30–60 day band was chosen because this frequency band is associated with 25–50% of the variance in the Kuroshio Extension (Greene et al. 2012). There is significant energy in the deep ocean within the 30–60 day band in POP, accounting for 20–30% of the variance agreeing with observations (Fig. 4c). Fig. 4b shows that the time series of $v_E'T'$, which is mostly the divergent component (Bishop et al. 2013), is also elevated during the CCR formation event. CCRs were associated with the largest DEHF events in KESS (Bishop 2013).

c. *Meridional Eddy Heat Transport*

The MEHT (Eq. 5) is shown in Figure 5 for KESS and POP. MEHT reaches a maximum value of 0.048 PW at 35.2°N and 0.055 PW at 35.5°N for KESS and POP respectively (1 PW = 10^{15} Watts). At their respective maximum values, MEHT from POP is 14% larger than KESS. POP's maximum MEHT is shifted poleward of the KESS observations by 0.3° latitude, which is due to the more northerly path of the Kuroshio Extension as mentioned earlier. This can be seen in Fig. 4a where the maximum fluxes are confined between the crest and trough at ∼35.5°N. The larger MEHT in POP is partly a manifestation of zonally-integrating over a less steep mean trough in POP (Figure 1). The mean trough in the path of the Kuroshio Extension has a steeper north-south extent in the KESS observations resulting in a smaller projection of the dominantly cross-stream DEHF vectors onto the meridional direction.

4. Discussion and Conclusions

The Kuroshio Extension jet axis in the 3 years of POP stayed in a more zonal path configuration within the first 1000 km east of Japan than is typically observed with satellite altimetry (seen from weekly contours of the Kuroshio Extension path not shown). Qiu and Chen (2005) observed from satellite altimetry decadal variability in the path of the Kuroshio Extension axis with transitions from high (unstable) to low (stable) variability linked to external forcing due to variations in the Pacific Decadal Oscillation (PDO). Despite the fact that POP is forced with annually-repeating winds, there is intrinsic interannual and decadal variability (Figure 6) not associated with PDO forcing. Douglass et al. (2012a) also pointed out that there is decadal variability in the formation of the Large Meander south of Japan. While the dynamics of these state transitions are beyond the scope of this study, the eddy statistics must be interpreted in the context of the mean flow state.

The KESS observations captured a transition from a stable to unstable path configuration in late 2004. The variability in KESS reflects the unstable period (Bishop 2013, 2012) with enhanced CCR formation and ring-jet interaction. The first year of the POP output (year 64) has a CCR that forms (Fig. 3). Figure 6 shows the time series of the area average over the KESS region of vertically-integrated EKE ($\frac{1}{2A}\int_A\int(u'^2+v'^2)dzdA$, where A is the area). EKE was elevated during the first year of the comparison period (model years 64–67) with the jet transitioning to a weaker meander phase thereafter, by coincidence, almost mirroring the KESS observations. See Figure 3 in Qiu and Chen (2010) for a comparison of EKE variability from observations with Figure 6, especially the transition from a low to high EKE state during KESS (June 2004–June 2006).

Even with these caveats, the 3 years of HR POP model data captures mean-to-eddy energy conversion rates and MEHT similar to observations during KESS. The horizontal and vertical structures from POP have a pleasing similarity to the KESS observations. There is crest-trough asymmetry in BC along the mean path in both KESS and POP. There is strong BC upstream of the mean trough with values that agree quantitatively to within 25%

with observations. The largest values are near the mean jet axis and peak in the horizontal along the 11°C isotherm and in the vertical near 400 m depth. The mechanism of vertical coupling, responsible for DEHFs in observations, are also shown to be present in POP. MEHT is comparable between KESS and POP with the peak in MEHT shifted northward in POP by $\sim$0.3° latitude, which is due to the more northerly path of the Kuroshio Extension jet. MEHT from POP is also higher by $\sim$14%.

For the first time observations of DEHFs with sufficient mesoscale resolution have been compared to a HR ocean model simulation. The level of agreement lends confidence to climate simulations using HR POP and suggests that HR POP can be used as a tool to validate parameterizations for mesoscale eddy processes within the Kuroshio Extension region. Other similar studies would need to be done to determine the utility of the model in other dynamically important regions. However, this study lends confidence to using POP to test parameterization schemes for mesoscale eddies used in non-eddy resolving global climate models.

Acknowledgments.

The authors thank Peter Gent and Justin Small for helpful comments that improved this manuscript. This work was supported under the Advanced Study Program at the National Center for Atmospheric Research (NCAR). NCAR is supported by the National Science Foundation.

REFERENCES

Bishop, S. P., 2012: The role of eddy fluxes in the Kuroshio Extension at 144°-148°E. Ph.D. thesis, University of Rhode Island.

Bishop, S. P., 2013: Divergent eddy heat fluxes in the Kuroshio Extension at 143°–149°E. Part II: Spatiotemporal variability. *Journal of Physical Oceanography*, accepted.

Bishop, S. P., D. R. Watts, and K. A. Donohue, 2013: Divergent eddy heat fluxes in the Kuroshio Extension at 143°–149°E. Part I: Mean structure. *Journal of Physical Oceanography*, **43**, 1533–1550.

Bishop, S. P., D. R. Watts, J.-H. Park, and N. G. Hogg, 2012: Evidence of bottom-trapped currents in the Kuroshio Extension region. *Journal of Physical Oceanography*, **42**, 321–328.

Chassignet, E. P. and D. P. Marshall, 2008: Gulf Stream separation in numerical ocean models. *Ocean Modeling in an Eddying Regime*, M. W. Hecht and H. Hasumi, Eds., American Geophysical Union, No. 177 in Geophysical Monograph Series, 39–61.

Cronin, M. and D. R. Watts, 1996: Eddy-mean flow interaction in the Gulf Stream at 68°W. Part I: Eddy energetics. *Journal of Physical Oceanography*, **26 (10)**, 2107–2131.

Donohue, K. A., D. R. Watts, K. L. Tracey, A. D. Greene, and M. Kennelly, 2010: Mapping circulation in the Kuroshio Extension with an array of current and pressure recording inverted echo sounders. *Journal of Atmospheric and Oceanic Technology*, **27 (3)**, 507–527.

Douglass, E. M., S. R. Jayne, F. O. Bryan, S. Peacock, and M. E. Maltrud, 2012a: Kuroshio pathways in a climatologically forced model. *Journal of Oceanography*, **68**, 625–639.

Douglass, E. M., S. R. Jayne, S. Peacock, F. O. Bryan, and M. E. Maltrud, 2012b: Subtropical Mode Water variability in a climatologically forced model in the northwestern Pacific Ocean. *Journal of Physical Oceanography*, **42**, 126–140.

Flierl, G. and J. C. McWilliams, 1977: Sampling requirements for measuring moments of eddy variability. *Journal of Marine Research*, **35 (4)**, 797–820.

Fox-Kemper, B., R. Ferrari, and J. Pedlosky, 2003: On the indeterminacy of rotational and divergent eddy fluxes. *Journal of Physical Oceanography*, **33 (2)**, 478–483.

Fox-Kemper, B., R. Lumpkin, and F. O. Bryan, in press: *Ocean Circulation and Climate - Observing and Modelling the Global Ocean*, chap. Lateral transport in the ocean interior. Elsevier.

Gent, P. R. and J. C. McWilliams, 1990: Isopycnal mixing in ocean circulating models. *Journal of Physical Oceanography*, **20**, 150–155.

Greene, A. D., D. R. Watts, G. G. Sutyrin, and H. Sasaki, 2012: Evidence of vertical coupling between the Kuroshio Extension and topographically controlled deep eddies. *Journal of Marine Research*, **70 (5)**, 719–747.

Hall, M. M., 1986: Assessing the energetics and dynamics of the Gulf Stream at 68°W from moored current measurements. *Journal of Marine Research*, **44**, 423–433.

Hecht, M. W. and H. Hasumi, (Eds.) , 2008: *Ocean Modeling in an Eddying Regime*. No. 177 in Geophysical Monograph Series, American Geophysical Union.

Jayne, S. R. and J. Marotzke, 2002: The oceanic eddy heat transport. *Journal of Physical Oceanography*, **32 (12)**, 3328–3345.

Jayne, S. R., et al., 2009: The Kuroshio Extension and its recirculation gyres. *Deep-Sea Research I*, **56**, 2088–2099.

Kirtman, B. P., et al., 2012: Impact of ocean model resolution on CCSM climate simuulations. *Climate Dynamics*, **39**, 1303–1328.

Large, W. G. and S. G. Yeager, 2009: The global climatology of an interannually varying air-sea flux data set. *Climate Dynamics*, **33**, 341–364.

Lenn, Y.-D., T. K. Chereskin, J. Sprintall, and J. L. McClean, 2011: Near-surface eddy heat and momentum fluxes in the Antarctic Circumpolar Current in Drake Passage. *Journal of Physical Oceanography*, **41**, 1385–1407.

Lindstrom, S., X. Qian, and D. R. Watts, 1997: Vertical motion in the Gulf Stream and its reltaion to meanders. *Journal of Geophysical Research*, **102**, 8485–8502.

Maltrud, M. E., F. O. Bryan, and S. Peacock, 2010: Boundary impulse response functions in a century-long eddying global ocean simulation. *Environmenal Fluid Mechanics*, **10**, 275–295.

Marshall, J. and G. Shutts, 1981: A note on rotational and divergent eddy fluxes. *Journal of Physical Oceanography*, **11 (12)**, 1677–1679.

McClean, J. L., M. E. Maltrud, and F. O. Bryan, 2006: Measures of the fidelity of eddying ocean models. *Oceanography*, **19 (1)**, 104–117.

McClean, J. L., et al., 2011: A prototype two-decade fully-coupled fine resolution CCSM simulation. *Ocean Modelling*, **39**, 10–30.

Phillips, H. E. and S. R. Rintoul, 2000: Eddy variability and energetics from direct current measurements in the Antarctic Circumpolar Current south of Australia. *Journal of Physical Oceanography*, **30 (12)**, 3050–3076.

Qiu, B. and S. Chen, 2005: Variability of the Kuroshio Extension jet, recirculation gyre, and mesoscale eddies on decadal time scales. *Journal of Physical Oceanography*, **35 (11)**, 2090–2103.

Qiu, B. and S. Chen, 2010: Eddy-mean flow interaction in the decadally modulating Kuroshio Extension system. *Deep Sea Research II*, **57**, 1090–1110.

Tracey, K. L., D. R. Watts, K. A. Donohue, and H. Ichikawa, 2012: Propagation of Kuroshio Extension meanders between 143°E and 149°E. *Journal of Physical Oceanography*, **42**, 581–601.

Watts, D. R. and K. L. Tracey, 2013: On identifying the divergent component of oceanic vector heat flux fields. *Journal of Physical Oceanography*, submitted.

List of Figures

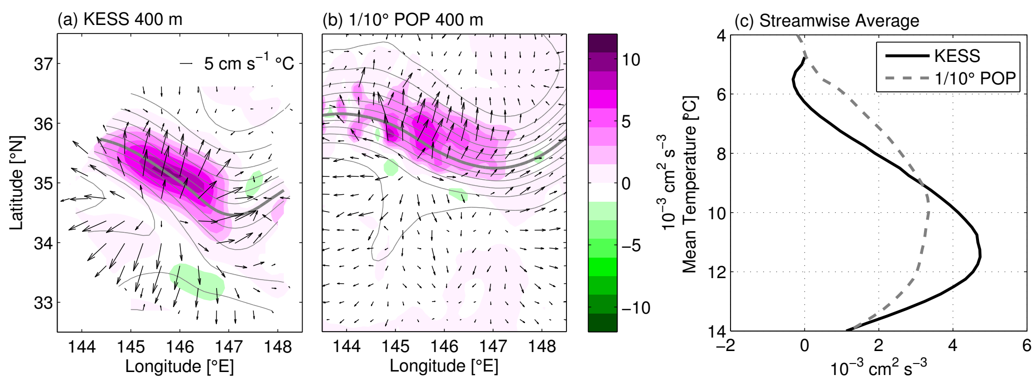

FIG. 1. Energy conversion rates, BC, at 400 m for (a) KESS (adapted from Bishop et al. (2013)) and (b) 0.1° POP. Superimposed are divergent eddy heat flux vectors every third grid point. Gray contours are mean temperature (ci = 1°C). The thick gray contour is the 11°C isotherm and representative of the jet axis. (c) BC in (a) and (b) averaged longitudinally along mean temperature contours.

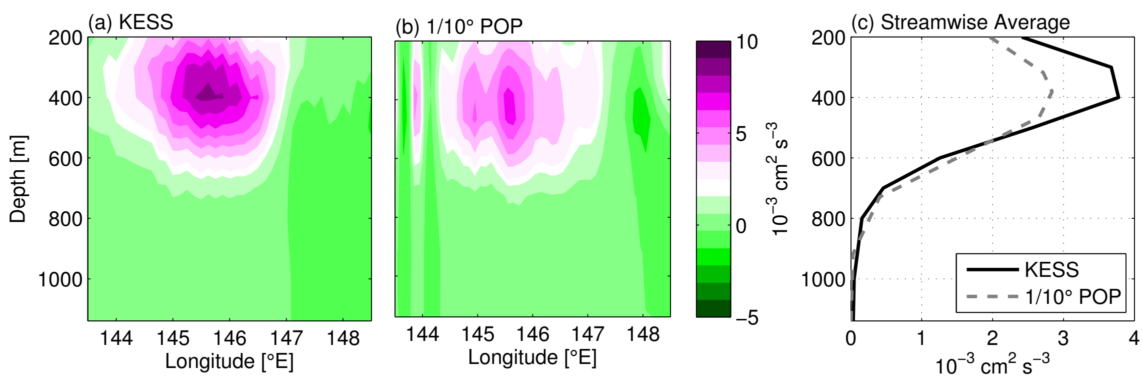

FIG. 2. Vertical structure of energy conversion rates, BC, for (a) KESS and (b) 0.1° POP as a function of longitude along the 11°C isotherm. (c) Longitudinal average of (a) and (b).

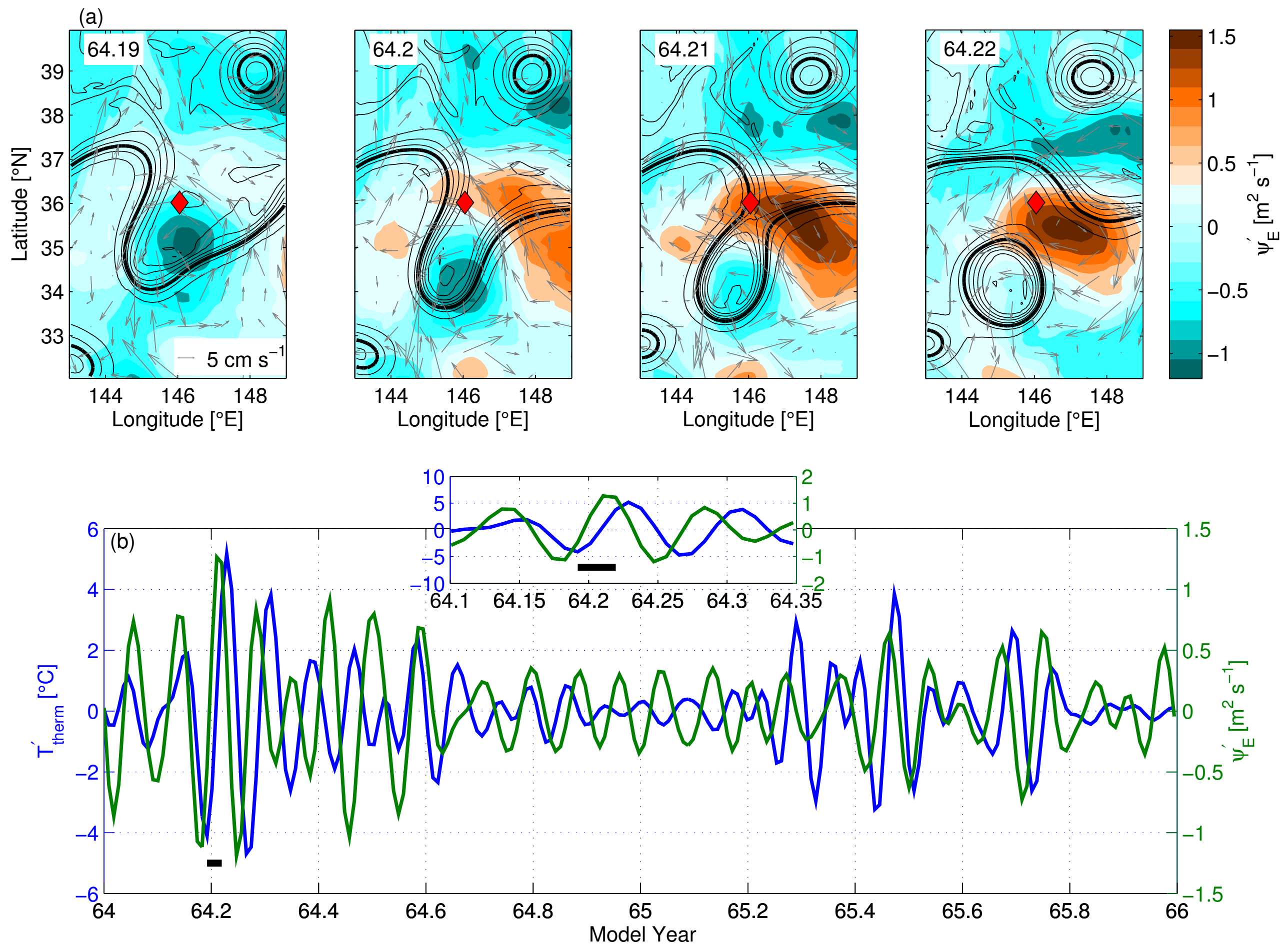

FIG. 3. Vertical coupling in the Kuroshio Extension in 0.1° POP. (a) Snap shots ever 5 days of the mid-thermocline temperature field at 381 m, T_{therm}, (black contours, ci = 2°C) during a CCR formation with the thick black contour marking the 12°C isotherm. Superimposed in color is the 30–60 day deep streamfunction, ψ'_E, at 5125 m (ci = 25 m^2 s^{-2}). The gray vectors are the 30–60 day deep current velocities at 5125 m plotted every sixth grid point. (b) 30–60 day mid-thermocline temperature at 381 m, T'_{therm}, in blue and the deep 30–60 day stream function, ψ'_E, in green at the location of the red diamond in (a). The inset is focused on the time around when the CCR formed in (a) with the thick black line marking the time interval in (a).

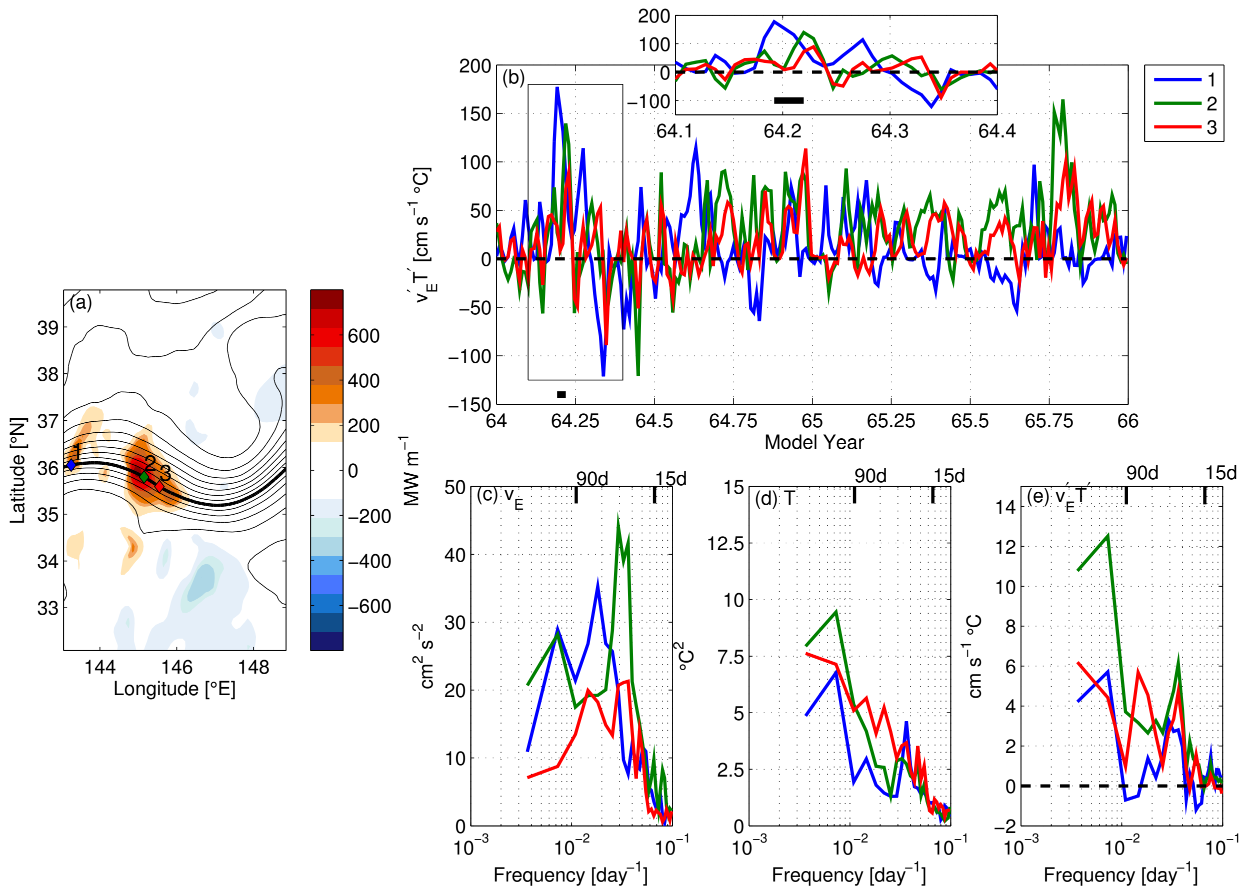

FIG. 4. (a) Vertically-integrated meridional eddy heat flux, $\rho_0 C_p \int_{-H}^{0} \overline{v_E' T'} dz$, (ci = 50 MW m^{-1}) with mean temperature contours at 381 m (ci = 1 °C). The thick black contour is the 12°C isotherm. (b) Time series of $v_E' T'$ at 381 m depth at the locations in (a). The thick black line marks the time when a CCR is forming in Fig. 3. (c)–(e) Variance-preserving power spectra of v_E, T at the mid-thermocline depth of 381 m, and cross-spectra of v_E and T respectively. Specta were estimated using the Welch method with a sampling frequency Fs = 1/5 cycles day^{-1}, segment length of 55 days, Hanning window, and 50% overlap.

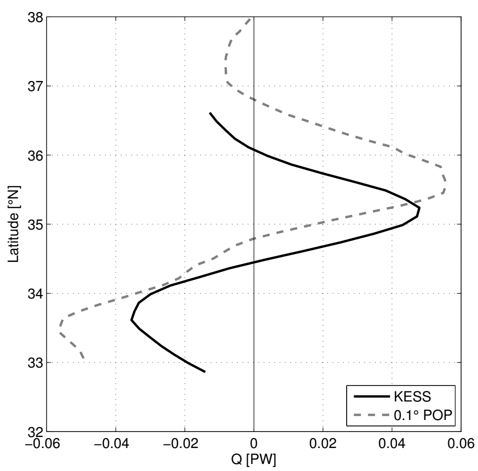

FIG. 5. Meridional eddy heat transport between 143.5°–148.5° for KESS and 0.1° POP.

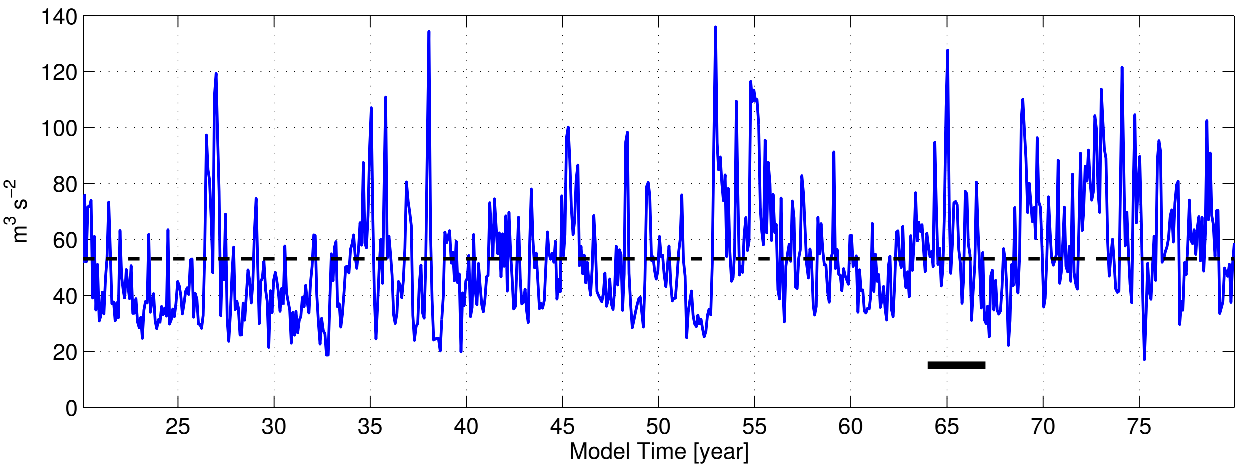

FIG. 6. Intrinsic decadal variability in 0.1° POP. Area average from 143°–149°E and 30°–40°N of vertically-integrated EKE time series for model years 20–80. The black dashed line is the average (53 $m^3 s^{-2}$) and the solid black line marks model years 64–67.